



Pauli paramagnetism of cubic V_3Al , $CrVTiAl$, and related 18-electron Heusler compounds with a group-13 element

Rui Zhang ^{*}, Zsolt Gercsi, M. Venkatesan, Karsten Rode , and J. M. D. Coey [†]
School of Physics, Trinity College Dublin, Dublin 2, Ireland



(Received 8 February 2021; accepted 19 April 2021; published 7 May 2021)

Calculations suggest that ordered Heusler alloys with 18 valence electrons could exhibit a variety of unusual electronic and magnetic states that are absent in the constituent elements. They include magnetic semiconductors, spin gapless semiconductors, compensated ferrimagnetic half-metals, and metallic antiferromagnets. Magnetic order has been predicted at exceptionally high temperature. Any of this would be of interest for spin electronics. Here, we investigate the magnetic properties of bulk, single-phase V_3Al , $CrVTiAl$ and the corresponding Ga compounds, with and without ^{57}Fe doping. Results are compared with data on the constituent elements. We conclude that all the as-cast alloys show some degree of B2-type ordering, but all of them are Pauli paramagnets with dimensionless susceptibilities close to the average of the atomic constituents. Prolonged annealing of the single-phase as-cast alloys leads to phase segregation. Density functional theory calculations on V_3X and $CrVTiX$ with $X = B, Al, Ga,$ and In confirm that different atomic arrangements on the four interpenetrating face-centered cubic sublattices of the Heusler structure could indeed lead to unusual magnetic properties, but both magnetism and semiconductivity are destroyed by disorder. The energy and entropy differences between different ordered magnetic phases preclude the stabilization of any single one of them. All are metastable and inaccessible in alloys prepared from the melt.

DOI: [10.1103/PhysRevB.103.174407](https://doi.org/10.1103/PhysRevB.103.174407)

I. INTRODUCTION

Heusler alloys are an enormous family of materials with four potentially distinct, interpenetrating face-centered cubic (fcc) sublattices in a cubic unit cell. The cell, composed of eight body-centered cubic (bcc) structural units, has a lattice parameter a_0 of ~ 600 pm. Discoveries of unexpected magnetic properties in this family [1] date back to the work of Heusler [2] on Cu_2MnSn , a ferromagnetic alloy that has no ferromagnetic component.

The structure is illustrated in Fig. 1; the four fcc sublattices are $4a$, $4b$, $4c$, and $4d$. Structures can be distinguished by the sequence of atoms W, X, Y, Z in the $4a$, $4c$, $4b$, $4d$ sites lying along a body diagonal. The origin can be chosen at any one of them. The Strukturbericht symbol and space group for the compounds are A2, $Im\bar{3}m$ (XXXX); B2, $Pm\bar{3}m$ (XYXY); DO_3 , $Fm\bar{3}m$ (XYYY); $L2_1$, $Fm\bar{3}m$ (XYXZ); XA, $F\bar{4}3m$ (XXYZ); and Y, $F\bar{4}3m$ (XWYZ). There are crystallographically distinct variants in each case except A2, depending on how the atoms are identified as WXY or Z. In the LiMg-PdSn Y-type structure, $4! = 24$ permutations of the atoms are possible on the four sublattices, but only three of them are crystallographically distinguishable. We denote them as I, II, and III. The order of the atoms along the diagonal in $CrVTiAl$, for example, can be I, Al-Ti-V-Cr; II, Al-Ti-Cr-V; or III, Al-V-Ti-Cr. The Y and XA structures have no center of inversion, but $L2_1$, DO_3 , B2, and A2 all have one.

It has been suggested by Skaftouros *et al.* [3] that many inverse XA Heusler alloys are half-metals, following the Slater-Pauling rule $m = n - 18$, where m is the moment per formula in Bohr magnetons, and n is the number of valence electrons in the formula (three for Al, Ga; four for Ti, V; and six for Cr, for example). This is analogous to the $m = n - 24$ Slater-Pauling rule that was established experimentally for $L2_1$ compounds, including the Co_2YZ series [1,3,4]. An extensive study by Ma *et al.* [5] of the calculated electronic structure of 127 such inverse Heuslers confirmed the presence of spin gaps and $n - 18$ half-metallicity. However, very few such materials have been realized experimentally, and none have < 26 electrons. The great majority have formation energy differences that are so small (50–100 meV/atom) with respect to other, stable phases or combinations of phases that they were thought unlikely to be synthesizable in equilibrium [5]. These formation energy differences are generally quoted with reference to the convex hull, which is an energy surface in compositional space, based on the energies of huge numbers of computed compounds archived in the AFLOWLIB or Open Quantum Materials (OQMD) databases. The hull distance is calculated as $\Delta E_{HD} = E_f - E_{hull}$, where E_{hull} is the energy of the convex hull, and E_f is the formation energy of a new phase. Stable phases lie on the hull ($\Delta E_{HD} = 0$), but when the hull distance ΔE_{HD} is positive, the phase is potentially unstable, and it could decompose into a combination of more stable compounds lying on the hull. Recent computational studies of binary, ternary, and quaternary Heuslers have tested potential new candidates for stability with respect to the hull [4–10].

The group-13 elements Al or Ga have eight spin-unsplit states at the bottom of the valence band arising from the

^{*}zhangr4@tcd.ie

[†]jcoey@tcd.ie

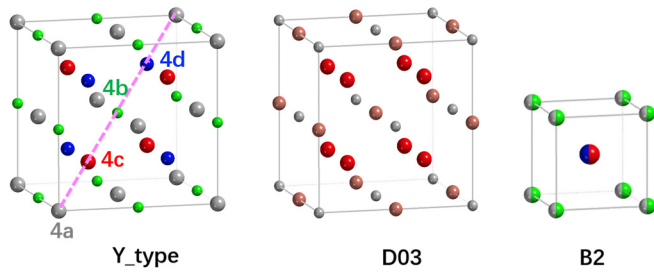


FIG. 1. An arrangement of four different atoms Cr, V, Ti, and Al on the four fcc sublattices along the body diagonal of the cubic Heusler Y-type structure. In the D0₃ structure, 4a is occupied by the group-13 element and 4b, 4c, and 4d sites are occupied V, whereas in the B2 structure, 4a and 4b sites are occupied by a mixture of elements and 4c and 4d sites by a different mixture. (In D0₃, the 4c and 4d sites are crystallographically equivalent and are referred to as 8c sites.)

3s/3p or 4s/4p orbitals, respectively. The nine 3d electrons may or may not occupy spin-split orbitals, with or without a gap at the Fermi level [11]. Some possible schematic densities of states (DOSs) are illustrated in Fig. 2, including one variety of spin gapless semiconductor [12]. The 18-electron compounds could be antiferromagnets or compensated ferrimagnets. Compensated ferrimagnetic semiconductors with different gaps in the \uparrow and \downarrow DOSs [13,14] are potential spin filters [15].

We first summarize density functional theory (DFT) calculations of the electronic structure of the 18-electron D0₃ and Y-type intermetallics. There have been several calculations for D0₃-V₃Al. (The low-temperature equilibrium phase is an A15 superconductor with $T_{sc} = 11.7$ K that becomes bcc above 600 °C [16].) First calculations found it to be a nonmagnetic gapless semiconductor [17]. Subsequently, it was identified as an antiferromagnetic (AFM) semiconductor [3,18]. Antiferromagnetism is possible because the vanadium on 4b sites has no moment, and the vanadium on the surrounding 8c sites forms two equivalent AFM coupled sublattices (4c and 4d) in a G-type spin structure, with moments of $\sim 1.5 \mu_B/\text{atom}$ and a calculated Néel temperature of 600–1000 K. The nonmagnetic state lies 0.039 eV/atom above the ordered AFM state [19]. Here, D0₃-type V₃Ga was calculated to be nonmagnetic [5] or else a G-type antiferromagnet [15,18] with a Néel temperature of 500–850 K. In both V₃Al and V₃Ga, a broad maximum in

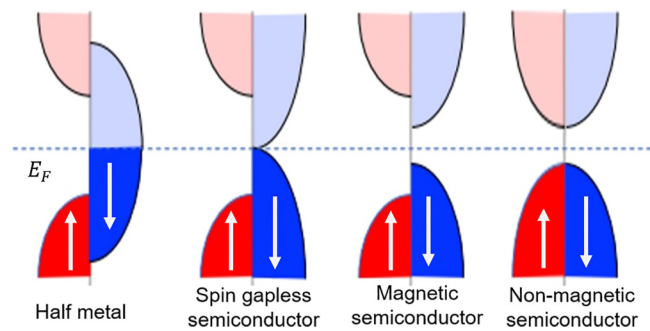


FIG. 2. Schematic densities of states suggested for zero-moment 18-electron Heusler compounds. The last panel can also represent an antiferromagnetic semiconductor.

the temperature dependence of magnetization is observed at 600 K [19] or 390 K [15], respectively, amounting to 1–2% of the susceptibility. The equilibrium phase for V₃Ga at these temperatures is A15 type.

The 18-electron quaternaries CrVTiAl and CrVTiGa were predicted to follow the XA ternary Heusler alloys and behave as fully compensated half-metallic ferrimagnets with a gap for one spin direction in the spin-polarized DOS. Calculations for CrVTiAl based on an ordered LiMgPdSn-type structure predicted a spin gap in both \uparrow and \downarrow DOS, and a magnetic ordering temperature $T_N > 2000$ K [13]. This is considerably higher than the value for cobalt, the metal with the highest known Curie temperature. There are equal and opposite moments on the Cr and V + Ti sublattices of $\sim 3 \mu_B$ but very little magnetism on Al [13]. On the basis of such electronic structure calculations, CrVTiAl was proposed as a spin filter for spin electronics [13,20] and as a spin gapless semiconductor where the spin gap in one band is practically zero [14]. The constituent elements behave quite differently. Three of them are Pauli paramagnets (Ti, V, and Al); the fourth (Cr) hosts an incommensurate AFM spin density wave arising from Fermi surface nesting with an amplitude of $0.43 \mu_B$ that is largely orbital in character. The Néel temperature T_N is 313 K [20].

The CrVTiAl alloy was subsequently prepared in bulk [14,20,21] and thin film form [22,23]. It crystallizes in a cubic structure with $a_0 \approx 610$ pm, and there is evidence of B2 atomic ordering [21,22]. The bulk alloy has a temperature-independent magnetic susceptibility $\chi = 4.5 \times 10^{-8} \text{ m}^3 \text{ kg}^{-1}$ with no sign of any net moment from 4–400 K according to one report [20]. In another report, the susceptibility is similar with a small upturn below 10 K [22], but evidence of a very small net moment of $10^{-3} \mu_B/\text{fu}$ and a little coercivity at 3 K together with some temperature dependence in the susceptibility at ~ 750 K were later attributed to an oxide impurity [22]. All samples studied showed a metallic residual resistivity ρ_0 in the range 160–280 $\mu\Omega \text{ cm}$. The temperature coefficient of resistance becomes negative at high temperature, which was interpreted as semiconducting behavior with a gap of 0.16 eV. The Hall coefficient is positive, consistent with hole densities of 10^{22} cm^{-3} . (The atom density in the compound is $7 \times 10^{22} \text{ cm}^{-3}$.) A small nonlinear component of magnetization observed in thin films saturates in ~ 2 T. These data were interpreted as showing that CrVTiAl is a fully compensated ferrimagnetic half-metal with a very high T_c . However, real materials are considered to exhibit a substantial degree of atomic disorder compared with the ideal structures in Fig. 1(a), and only a small fraction of any sample was estimated to be in a fully ordered Y structure or one with only Cr/V disorder, both of which exhibit spin gaps [14].

To our knowledge, there is no publication on these materials showing direct evidence of magnetic ordering such as magnetic neutron diffraction, anomalous Hall effect, or measurement of magnetic hyperfine interactions. Nor are there data showing hysteresis measured by the magneto-optic Kerr effect, domains, or spin-torque switching such as have been reported in Mn₂Ru_xGa, the most thoroughly studied example of a compensated half-metal [24]. Nevertheless, absence of evidence is not evidence of absence.

Our primary aim here is to investigate the magnetism of the 18-valence electron D0₃- and Y- structure Heusler

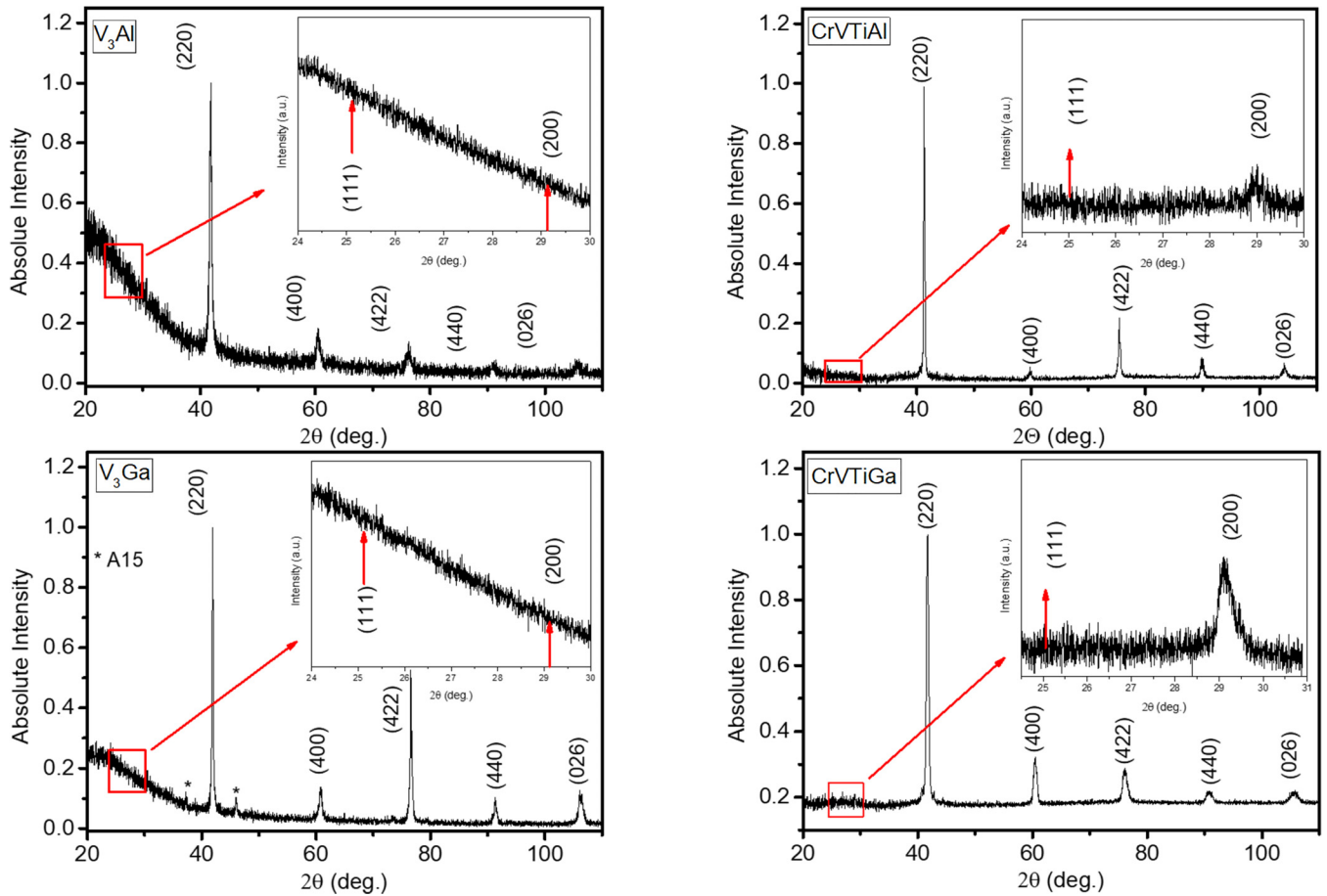


FIG. 3. X-ray diffraction patterns of as-cast alloys: V_3Al and V_3Ga (left) and $CrVTiAl$ and $CrVTiGa$ (right).

compounds experimentally to see whether they fulfill any of the interesting theoretical predictions. Materials selected for the study are bulk V_3Al and $CrVTiAl$, together with their Ga counterparts. Samples doped with 1 wt % of ^{57}Fe are included for Mössbauer spectroscopy. Then we explore and discuss the dependence of magnetism on atomic order in the four sublattices using DFT calculations, which are extended to cover two other group-13 elements, B and In. We find that the G-type AFM spin arrangement is a generic feature of the 18-electron DO_3 series. The stability of the magnetically ordered configurations is investigated in the binary and quaternary series as

well as the stability of the atomic order and the structures themselves.

II. EXPERIMENTAL RESULTS

Alloys were prepared by arc melting the elements (99.99% pure) Cr, V, Ti, and Al or Ga under argon. Samples were also prepared with 1 wt % of ^{57}Fe . The alloys were first studied in the as-cast state and then after annealing for 10 d in vacuum at 650 or 900 °C followed by furnace cooling or quenching to ambient temperature. Some representative x-ray diffraction

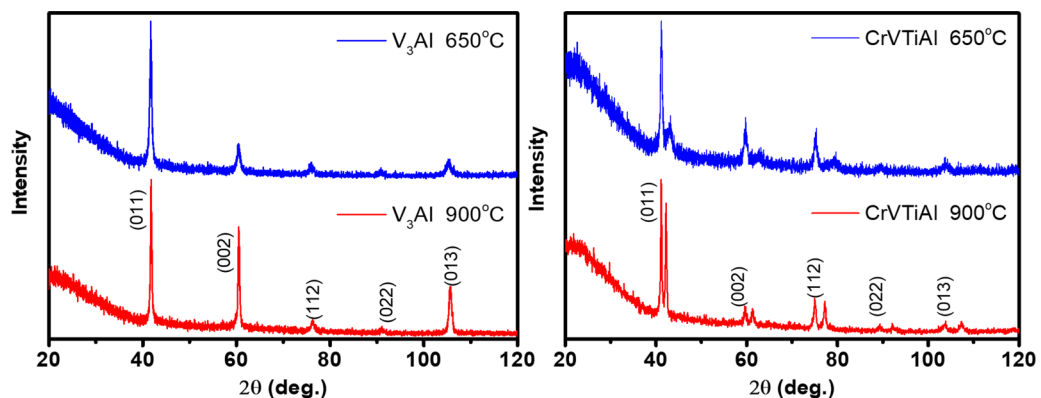


FIG. 4. X-ray diffraction patterns of as-cast alloys after annealing at 650 or 900 °C.

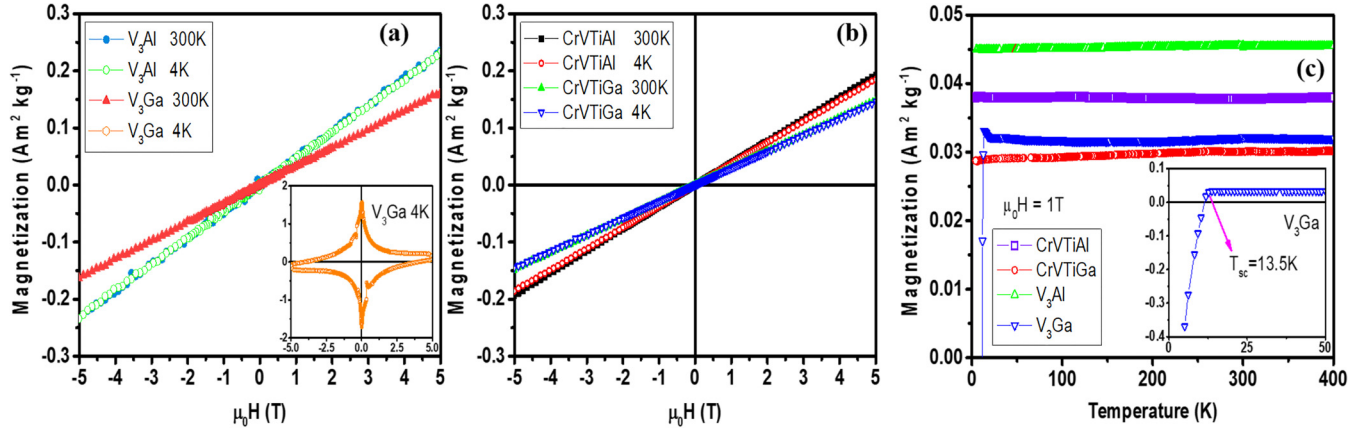


FIG. 5. Magnetization data. Field variation at 4 K and 300 K for (a) V_3Al/Ga and (b) $CrVTiAl/Ga$. (c) Temperature scans of the susceptibility in 0.5 T.

data for as-cast material are shown in Fig. 3. All the as-cast alloys were single phase, except for V_3Ga , which showed a trace of an A15 Cr_3Si -structure secondary phase. The main peaks in all cases correspond to the A2 bcc structure, but a weak 200 reflection found in all of them indicates some tendency toward B2 atomic order. The x-ray diffraction patterns of the ^{57}Fe -doped samples were no different. There was no sign of a (111) reflection, which is a marker for DO_{3-} , L_{21-} , $XA-$, and Y -type order, even after long counts around $2\theta = 25^\circ$. Data are included in Fig. 3.

Analysis of the ratio of the 002/004 peak heights [25] for $CrVTiAl$ compared with the ratio of the 001/002 peak heights for B2-ordered $(V + Cr)/(Ti + Al)$ allowed the degree of B2 order to be quantified as $S_{B2} = 0.46$. The corresponding result for the Ga alloys is $S_{B2} = 0.41$. Estimated errors are ± 0.05 . The as-cast alloys are therefore partly ordered at the level of the bcc subcell but not at the level of the $8\times$ larger Heusler cell (Fig. 1).

Prolonged annealing of the as-cast ingots at 650 or 900 $^\circ C$ failed to improve the atomic order. On the contrary, the as-cast single cubic phase with partial B2 order disproportionated into two or more separate cubic phases with different lattice parameters. The example of $CrVTiAl$ is shown in Fig. 4. From differential scanning calorimetry (DSC) at 10 $^\circ C$ per minute, the phase segregation is found to occur in the range 400–500 $^\circ C$. The quaternary appears to decompose into VCr and $TiAl$ solid solutions, with lattice parameters of 295 and

TABLE I. Lattice parameter, x-ray density, and susceptibilities of the as-cast alloys.

Compound	a_0 (pm)	ρ (kgm^{-3})	χ_m ($10^{-9} m^3 kg^{-1}$)	χ (10^{-6})
$CrVTiAl$	617	5042	44.8	226
$CrVTiAl$ (^{57}Fe)	614	5115	33.8	173
$CrVTiGa$	612	6389	37.1	237
$CrVTiGa$ (^{57}Fe)	611	6435	37.0	238
V_3Al	608	5311	56.5	300
V_3Al (^{57}Fe)	610	5360	57.7	309
V_3Ga	(605)	6669	41.3	275

309 pm, respectively. The phase segregation temperature for $CrVTiGa$ was a little higher.

V_3Ga was different. It showed a trace of A15-structure impurity already in the as-cast state, and annealing at 650 or 900 $^\circ C$ transformed it completely into the A15 structure, as anticipated from the phase diagram. Refinement of the structure in the space group $Pm-3n$ gives $a_0 = 462.1$ pm and a composition of $V_{2.9}Ga$. A15-type V_3Al was not obtained after these anneals.

Magnetization data are presented in Fig. 5 for as-cast, single-phase samples. In every case, the magnetization is linear in the field of up to 5 T at temperatures ranging from 4 to 400 K. The ^{57}Fe -doped samples behave similarly. There is no sign of any weak moment, and the susceptibility is temperature independent to within ± 1 . Changes seen at higher temperatures up to 900 K were irreversible and associated with phase segregation. They amount to $< 2\%$ of the room-temperature susceptibility.

Only V_3Ga behaves differently. Due to the trace of the superconducting A15 phase in the alloy, it exhibits a Meissner effect below $T_{sc} = 13.5$ K [Figs. 5(a) and 5(c) inserts]. From the initial negative susceptibility of -0.031 at 4 K, the volume fraction of A15 in the as-cast sample is estimated as 3%.

Table I summarizes the lattice parameters, x-ray density, mass susceptibility, and dimensionless susceptibility for the as-cast 18-electron alloys. The magnitude of the temperature-independent paramagnetic moment in 5 T lies in the range 1.0×10^{-3} to $1.5 \times 10^{-3} \mu_B$ per atom. Values of the dimensionless susceptibility χ for the alloys fall $\sim 40\%$ short of the value required for the appearance of spontaneous

TABLE II. Density and susceptibility of the pure elements [31].

Element	Structure	ρ (kgm^{-3})	χ_m ($10^{-9} m^3 kg^{-1}$)	χ (10^{-6})
Al	fcc	2698	7.7	21
Ga	ortho.	5907	-3.9	-23
Ti	hcp	4540	40.1	182
V	bcc	6110	62.8	384
Cr	bcc	7190	44.5	320

TABLE III. Comparison of the dimensionless susceptibility of the compounds with the averaged values of the constituent elements.

Compound	χ_{av} (10^{-6})	χ (10^{-6})
CrVTiAl	227	226
CrVTiGa	216	237
V ₃ Al	293	300
V ₃ Ga	282	275

ferromagnetism according to the Stoner criterion [26]. The susceptibility of the 1% iron-doped alloys was likewise temperature independent down to 4 K.

Values of density and susceptibility for the pure elements are provided in Table II for comparison. It is remarkable that the volume-averaged dimensionless susceptibility of the elements χ_{av} agrees very well with the measured susceptibility of all four alloys (Table III). Furthermore, the susceptibility of vanadium is temperature independent below room temperature [27], and that of chromium is temperature independent above the Néel temperature and decreases by 4% at lower temperatures [28]. The susceptibility of bcc VCr [29] and VTi [30] solid solutions shows little temperature dependence as well.

No evidence of any reversible AFM transition in V₃Al or V₃Ga was observed in DSC in the range 30–1000 °C, where compounds were thought to order antiferromagnetically [15,19]. Instead, there is an irreversible exothermic transition at 380 °C for V₃Al, which is associated with a very small, irreversible decrease in susceptibility at the same temperature. In V₃Ga, there is a larger exothermic transition at 490 °C, which is associated with the irreversible transformation to the A15 structure. In the quaternaries, we find exothermic events at 445 °C for CrVTiAl and at 505 °C for CrVTiGa, where the irreversible phase segregation takes place. A small (~2%) irreversible step appears in susceptibility at the same temperature.

A direct probe of any magnetic order is provided by Mössbauer spectroscopy of 1% ⁵⁷Fe-doped samples. There is no perceptible difference in the x-ray patterns in the samples with or without 1% of iron, and only minor changes are found in

the magnetic susceptibility (Table I). The room temperature spectra of the iron-doped alloys shown in Fig. 6 indicate that the iron is paramagnetic, with an isomer shift of -0.14 mm s⁻¹ with respect to the source ⁵⁷Co in Rh. The quadrupole splitting of 0.42 mm s⁻¹ for CrVTiAl and CrVTiGa [Fig. 6(a)] reflects a range of disordered atomic environments for the ⁵⁷Fe impurity. In V₃Al [Fig. 6(b)], there is also an unsplit central peak which is due to ~20% of the iron that is situated in a locally symmetric nearest neighbor environment. There is no magnetic hyperfine splitting in any of the alloys; the hyperfine field is <1T. We conclude that none of the alloys are magnetically ordered at room temperature.

III. ANALYSIS AND ELECTRONIC STRUCTURE CALCULATIONS

In view of the theoretical predictions of unusual gapped electronic structures and high magnetic ordering temperatures in the atomically ordered 18-electron compounds, we should consider what magnetic susceptibility could be expected. The order would have to be AFM with chemically identical sublattices because, as pointed out by Şaşıoğlu [32], a ferrimagnetic half-metal will exhibit compensation only at a specific compensation temperature, which will be $T_{comp} = 0$ K when the ground state is fully compensated. Atoms on the chemically or crystallographically distinct sublattices experience different exchange interactions, and therefore, the temperature dependence of the two sublattice magnetizations will generally be different. This is the behavior found in thin films of the 24-electron Heusler half-metal Mn₂Ru_{0.5}Ga (assuming no vacancies) [33–35], which can exhibit compensation at $T = 0$ K but has a nonzero net moment at other temperatures. The 24-electron bulk Heusler Mn_{1.5}V_{0.5}FeAl behaves similarly [34]. None of the binary V₃X or quaternary CrVTiX alloys exhibit spontaneous magnetization at any temperature.

A. Molecular field theory

It might be argued that a very high Néel temperature could account for the linear and practically temperature-independent magnetization curves. In the molecular field theory of a polycrystalline antiferromagnet, the low temperature susceptibility

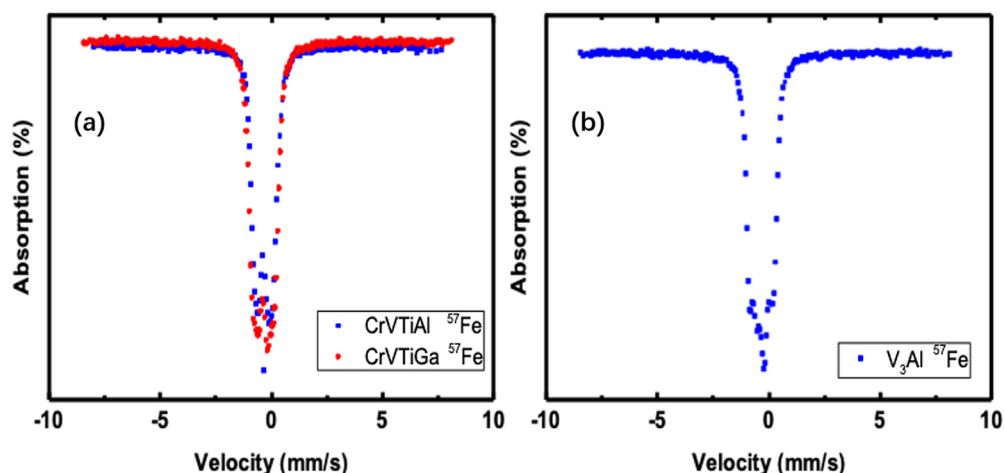


FIG. 6. ⁵⁷Fe Mössbauer spectra of 1 wt % iron impurities in (a) CrVTiAl and CrVTiGa and (b) V₃Al.

$\chi(0)$ is two-thirds of the value at T_N ; the intersublattice Weiss constant $n_{AB} = 1/\chi(T_N) = 2/[3\chi(0)]$ [26]. In our materials $\chi(0) = \chi \approx 232 \times 10^{-6}$ for CrTiVAl/Ga and $\chi \approx 288 \times 10^{-6}$ for $V_3\text{Al}/\text{Ga}$ (Table I). Hence, $n_{AB} \approx 2874$ in the first case and 2315 in the second. The sublattice moments found in DFT calculations are $\sim 3 \mu_B/\text{atom}$ in the quaternaries and $2 \mu_B/\text{atom}$ in the binaries. The respective sublattice Curie constants $C' = \mu_0 N m_{\text{eff}}^2 / 6k_B$ are 0.73 and 0.38 K, respectively, so the corresponding Néel temperatures $T_N \approx C' n_{AB}$ necessary to explain the small temperature-independent susceptibilities we observe would be 2098 and 880 K. In other words, a localized moment quaternary antiferromagnet with a reasonable Néel temperature of < 1000 K (see below) would have to have a susceptibility twice as large as those we observe. If that were true, the metallic alloys would satisfy the Stoner criterion and become spontaneously ferromagnetic.

From the expression for the Pauli susceptibility χ_P in terms of $\mathcal{N}(E_F)$, the DOS (both spins) at the Fermi level $\chi_P = \mu_0 \mu_B^2 \mathcal{N}(E_F)$, where μ_B is the Bohr magneton, we deduce that $\mathcal{N}(E_F) \approx 2.4 \times 10^{48}$ states/J/m³ or 5 states/eV/atom. The large DOS at the Fermi level is incompatible with a semiconductor. Substantial scattering due to atomic disorder may account for the large residual resistivities of $\sim 200 \mu\Omega$ cm observed in Refs. [14,22].

B. DFT calculations

Ab initio calculations based on DFT calculations were carried out using norm-conserving pseudopotentials and pseudo-atomic localized basis functions as implemented in the OPENMX software package [36]. The Y-type ordered calculations were based on a minimal 4-atom basis cell of the Heusler structure using $15 \times 15 \times 15$ k-points to evaluate the total energies. The conventional 16-atom basis cell was used for the investigation of antisite (V-X) swapping in the binary V_3X alloys. Pregenerated fully relativistic pseudopotentials and the pseudo-atomic orbitals with a cut-off radius of 7 atomic units (au) were used with *s2p2d2* for the metal and *s2p2d1* basis orbitals for the group-13 metalloid elements with an energy cutoff of 220 Ry (3 keV) for the numerical integrations. The convergence criterion for the energy minimization procedure was set to 10^{-8} Hartree (4 μeV). Spin-orbit interaction was not considered in the calculations. These conditions were tested on other previously reported full Heusler alloys, and excellent reproducibility was confirmed. The plotted DOSs were evaluated on a denser ($19 \times 19 \times 19$) k-grid for more detail.

TABLE IV. Calculated lattice parameters and vanadium magnetic moments on ordered D_{03} -type V_3X alloys with $X = B, \text{Al}, \text{Ga},$ and In (columns 2 and 3) compared with the Al antisite defect counterparts having a single Al atom on a $4b$ site (column 5) or an $8c$ site (column 7) in the 16-atom cell. AFM, antiferromagnetic; AFS, antiferromagnetic semiconductor; FiM, ferrimagnetic metal; NM, nonmagnetic.

	a_0 (pm)	m (μ_B)	Band structure	m_{4b} (μ_B)	Band structure	$m_{8c} - m_{\text{total}}$ (μ_B)	Band structure	Stable phase	Hull distance (eV/atom)
V_3B	571	0.90	AFS	0	Metallic/NM	0	Metallic/NM	$V_3B_2 + V$	0.486(D_{03})
$V_3\text{Al}$	612	1.62	AFS	1.10	Metallic/AFM	1.26	Metallic/FiM	$\text{AlV}_2 + V$	0.011(A15) 0.1333(D_{03})
$V_3\text{Ga}$	613	1.63	AFS	1.20	Metallic/AFM	1.68	Metallic/FiM	$V_3\text{Ga}$ (A15)	0.1642(D_{03})
$V_3\text{In}$	636	1.96	AFS	1.79	Metallic/AFM	1.24	Metallic/FiM	$\text{In} + V$	0.218(D_{03})

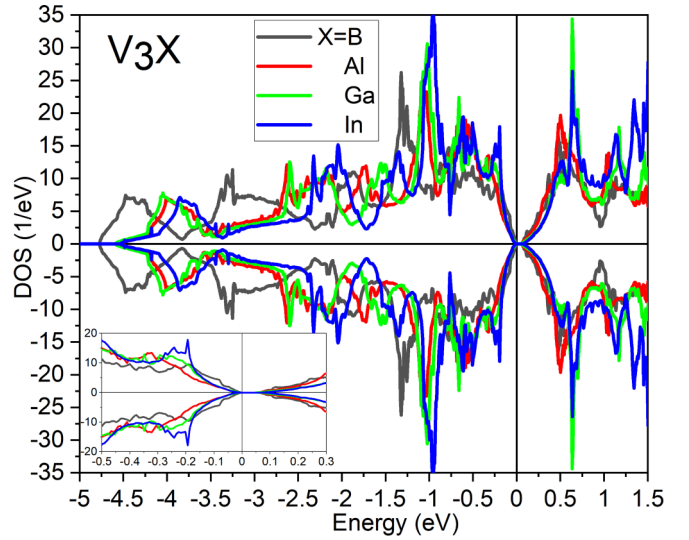


FIG. 7. Calculated densities of states for the 18-electron anti-ferromagnetic D_{03} -type V_3X binary alloys with different group-13 elements.

1. Binary V_3X compositions

We begin with the 18-electron binary V_3X compositions, where X is a group-13 element with a nominal valence of three. Calculations for compositions with D_{03} -type order and $X = \text{Al}, \text{Ga},$ and In have shown a striking dual magnetic nature of vanadium in the structure [18]. Our calculations, which also include $X = B$, confirm that vanadium atoms at the $8c$ sites are AFM coupled to each other with magnetic moments of $1.4\text{--}1.7 \mu_B$, while there is no magnetic moment on vanadium at the $4b$ site, which is surrounded by a cube of $8c$ sites occupied by the AFM ordered vanadium. The ordered D_{03} alloys are predicted to be AFM semiconductors.

The common behavior of all the binaries, regardless of the element X , is illustrated in Fig. 7. The total DOSs at 0 K share similar features: a symmetrical electronic structure in respect to spin-up and spin-down channels, with a narrow 100 meV energy gap above a filled valence band. The optimized lattice parameters a_0 and the calculated magnetic moments at the $8c$ and $4d$ vanadium sites are listed in Table IV. We find that the amplitude of the magnetic moment directly mirrors the atomic separation; the larger the atomic radius of X , the larger the magnetic moment on the $8c$ vanadium in column 3. This is because the degree of *p-d* orbital hybridization of the vanadium *d* electrons with the X valence *p* electrons

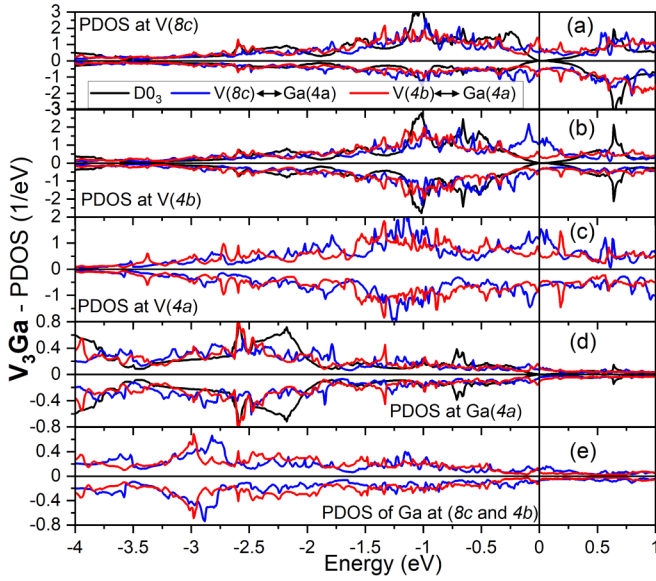


FIG. 8. Site-resolved partial densities of states in V_3Ga , showing the consequences of Ga antisite defects.

is similar across the series, but the exchange increases with lattice parameter.

We illustrate the electronic structure found in the series by plotting the DOS for V_3Ga in Fig. 8. First, we look at the partial DOS for the perfectly ordered $D0_3$ atomic structure, drawn in black in Figs. 8(a), 8(b), and 8(d); well-defined peaks are observed for all three sites. The symmetrical peaks in up- and down-spin states for both V and Ga in $4b$ and $4a$ positions is evidence of their nonmagnetic character. The only exchange-split partial DOS is for V at the $8c$ site.

The predicted AFM state with a gap at the Fermi level is a result of the highly idealized atomic arrangement. We found experimentally, even when a single-phase B2 structure is formed, that there is a high degree of atomic site disorder, which is inimical to AFM semiconductivity. In Figs. 8(a)–8(e), we illustrate the impact of the two possible sorts of atomic disorder: Ga($4a$) antisite swapping with V($4b$) or V($8c$). The delicate electronic and magnetic balance of the G-type AFM structure on the $8c$ site collapses with a single Ga replacement on a vanadium sublattice site. Interestingly, as can be seen in Fig. 8(a), every remaining V($8c$) atom contributes new electronic states at E_F , not only the substitutional Ga. The weight of the partial DOS of the substitutional Ga is shifted to -1 eV and above, where stronger p - d hybridization takes place [Fig. 8(d)]. This effect reduces the V($8c$) magnetic moment to $\sim 0.9 \mu_B$ with an unbalanced number of spins.

TABLE V. Calculated electronic states of Y-type variants in CrVTiX compounds, together with the hull distance of the most stable variant. HM, half-metal; NM, nonmagnetic; FiM, ferrimagnetic; SGS, spin gapless semiconductor.

CrVTiX	I	II	III	Stable phases	Hull distance (eV/atom)
B	Metallic	NM metallic	SGS (spin filter)	TiB + V_3B_2 + TiCr ₂ + Ti	0.465 (Y–III)
Al	HM	FiM metallic	SGS (spin filter)	TiAl + VCr	0.114 (Y–III)
Ga	HM	FiM metallic	SGS (spin filter)	TiGa + VCr	0.125 (Y–III)
In	HM	FiM metallic	SGS (spin filter)	TiIn + VCr	0.238 (Y–III)

In addition, the vanadium exchanged to the $4a$ site develops a small moment of $\sim 0.2 \mu_B$. The net ferrimagnetic moment is $\sim 1.1 \mu_B$ /fu. There is a similarly big impact of the $4b$ site Al atom on the electronic structure, but the number of reduced moments is still in balance to make up for a complete AFM type coupling with $m = 0 \mu_B$ /fu. These results are all summarized in Table IV. Our description was for V_3Ga , but the conclusion for antites with $X = Al$ and In are very similar. Our results for $D0_3$ -ordered V_3Al are in accord with those of Kuroda *et al.* [6], but atomic disorder significantly weakens the magnetic interactions and destroys the semiconducting character of the compound. For V_3B , the one with the smallest lattice parameter, the magnetic moment on V($8c$) also collapses to give a nonmagnetic metallic electronic structure because of any boron antisites. The magnetic balance in the case of V_3B results in the disappearance of collective magnetism in this composition regardless of any atomic site disorder.

2. Quaternary CrVTiX compositions

Although the 18-electron binaries do exhibit antiferromagnetism when they have complete $D0_3$ -type atomic order, the electronic structure manifested in symmetrical spin channels (Fig. 1) offers no benefits for spintronic applications. Further alloying elements are needed to transform the $D0_3$ -type order into a possible XA- or Y-type atomic arrangement. Such alloys might be created by partial replacement of V by other transition metal elements, but to retain the desired balance of 18 electrons and zero net moment, a simultaneous replacement of two vanadium atoms by a chromium and a titanium is needed. This alloying approach could yield a ferrimagnetic spin structure with asymmetric spin states at the Fermi level, as predicted for CrVTiAl [13,22,23]. The Y-type alloy can order in any one of the three inequivalent atomic arrangements described in the Introduction [37], which display strikingly different electronic structures ranging from metal to spin gapless semiconductor to half-metal (see Table V). In addition, all these states appear in a fully compensated ferrimagnetic spin arrangement at $T = 0$.

Here again, we extend the study beyond CrVTiAl to 18-electron quaternaries with B, Ga, or In. To investigate the relative stability of these phases, we first establish the total energy differences for the three possible variants in Fig. 9. Except for CrVTiB, a ferrimagnetic variant is found to be slightly more favorable than a nonmagnetic one. We observe the same trend that $E_{tot}(III) < E_{tot}(I) < E_{tot}(II)$ at the lowest energy point in cubic parameter space for the magnetic solutions. Variant (III) suggests a preferential high-spin state of Cr and V, as plotted in Fig. 10. The large moments of 2.9 – $3.6 \mu_B$

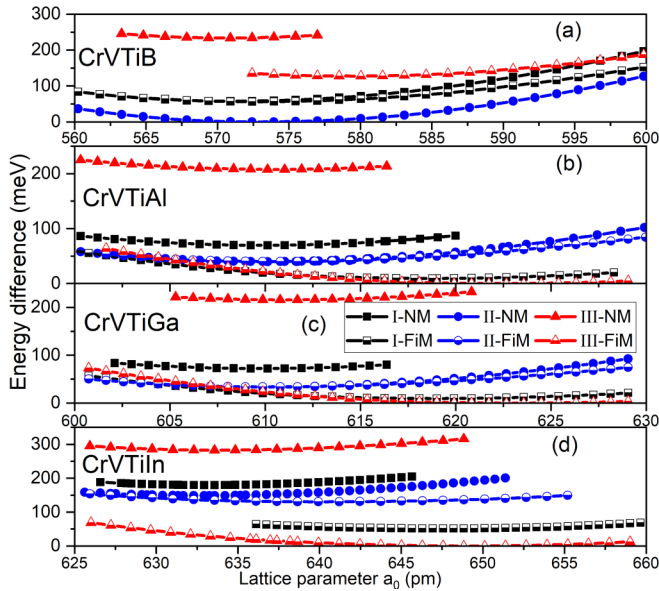


FIG. 9. Energies of the three variants (I, II, and III) of the quaternary CrVTiX alloys, as a function of lattice parameter distinguishing ferrimagnetic and nonmagnetic solutions.

for Cr are counterbalanced by a moment of $2\text{--}3 \mu_B$ on V, with the difference being made up by a small moment ($0.5\text{--}1.5 \mu_B$) on the Ti to arrive at $m = 0 \mu_B/\text{f.u.}$ Similarly, large moments are found on the Cr and V sites in variant II. On the other hand, energetically unfavorable nonmagnetic states with a metallic band structure are found for variant I.

In view of the role of atomic separation in binary V_3X compositions, we can understand the lack of stable magnetism in the quaternary CrVTiB compound. The boron in the Y-type structures results in significant overlap of p orbitals of B with d orbitals of the transition metals Ti, V, and Cr, resulting in broad hybrid orbitals that do not sustain spontaneous magnetic moments. Larger metalloid sizes expand the atomic separations, allowing stable magnetic moments to develop. However, the picture that emerges for $X = \text{Al}$ and Ga from Figs. 9(b) and 9(c) is of competing magnetic and nonmagnetic phases with different lattice parameters and energy differences of tens of meV, barely greater than ambient temperature.

The magnetic and nonmagnetic versions of variant III have quite different energy and lattice parameters. Although the former might have a high magnetic ordering temperature if it could be realized [13], the practical difficulties to achieve a fully relaxed highly ordered single-variant quaternary atomic structure from the melt seem insurmountable. The close vicinity in energy of variants I, II, and III, some of them differing in energy by $<25 \text{ meV}$ ($k_B T$ at ambient temperature), suggests that a disordered high-entropy alloy will form rather than an ordered quaternary phase [38]. High-entropy alloys are defined, somewhat arbitrarily, as having five or more approximately equal atomic components [39]. They can have remarkable mechanical properties [40,41], but there is little benefit from mixing magnetic and nonmagnetic atoms together in terms of useful magnetic functionality. Entropy always tends to favor atomic disorder in quaternary alloys rather than intermetallic compound formation. A free energy of $\ln 4 \times k_B T$ per atom is gained from complete disorder, which amounts to 50 meV/atom at 420 K , hindering formation of atomically and magnetically ordered structures.

Worst of all, none of the ordered phases that we have discussed at some length is thermodynamically stable. They all tend to decompose into the phase mixtures noted in Tables IV and V. The fundamental contradiction between theory and experiment hinges on the stability of a single cubic phase before any degree of order can be considered. Ma *et al.* [4,5] emphasized this point in their analysis of hundreds of ternary XA or $L2_1$ alloys, comparing the energies of ordered cubic Heusler alloys with the energies of mixtures of potential competing phases that can be found on the hull in the large OQMD public database [42,43] to estimate the likelihood that an ordered Heusler phase is thermodynamically stable. When the energy distance from the convex energy curve in compositional space connecting the most stable mixtures of phases is $<50\text{--}100 \text{ meV/atom}$, the phase may be regarded as unlikely to form in practice. We have indicated the calculated hull distances together with the stable phases in competition for both series of binary and quaternary alloys in Tables IV and V. The one binary that is stable is A15 $V_3\text{Ga}$. For $V_3\text{Al}$, there is no single stable binary phase, although $D0_3$ and A15 come close. Our experiments are in full agreement with this prediction. Furthermore, both $V_3\text{B}$ and $V_3\text{In}$ are

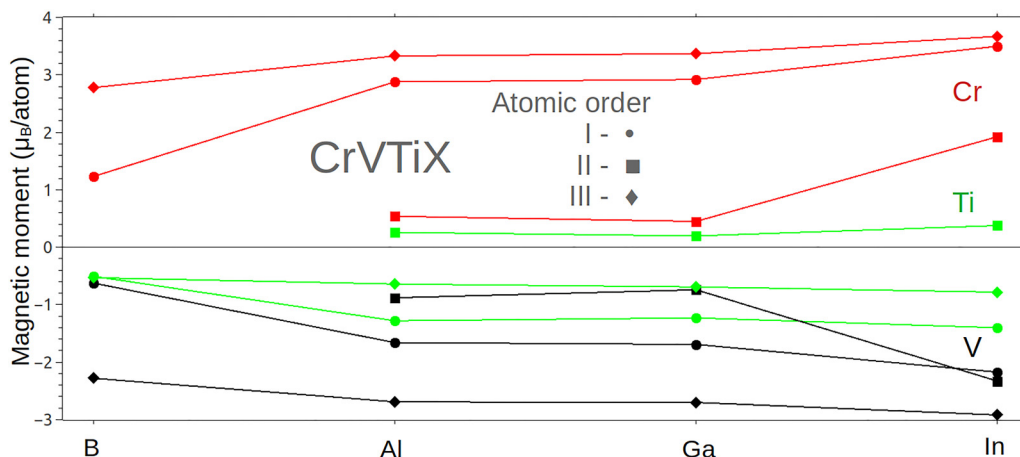


FIG. 10. Atomic magnetic moments on Cr, Ti, and V in ordered CrVTiX, $X = \text{B}$, Al, Ga, and In.

highly unstable, with a strong tendency to phase separation in the case of B and complete immiscibility in the case of In.

The Al and Ga compounds are also the best candidates in the quaternary series, with formation energies closest to the hull, justifying our selection of them for the study. However, our experiments confirm that annealing as-cast material in the hope of achieving a higher degree of atomic order is doomed to fail because two-phase decomposition is a lower energy solution.

IV. CONCLUSIONS

This paper illustrates the caution that is needed when attempting to relate the results of DFT calculations to bulk materials that can be made in a laboratory or a production line. The calculations confirm that the four idealized D0₃-ordered binary vanadium phases can be AFM semiconductors with nonmagnetic vanadium on 4*b* sites. Unfortunately, low energy antisite defects eliminate the semiconductivity and tend to destroy the magnetism. In the case of the Y-phase quaternary alloys, differently ordered variants with or without magnetic order differ in energy by such a small amount, 50 meV/atom or less, that it is practically impossible to separate them. Entropy contributes further to the atomic disorder in what are effectively high-entropy alloys.

Furthermore, a fully ordered D0₃ binary or any Y-type quaternary variant is not the most stable solution for any of these compounds. There are combinations of phases which lie on the hull with a lower energy. No method of synthesis that requires melting of the constituents will succeed in producing the 18-electron Heusler compounds with the spin gaps at the Fermi level illustrated in Fig. 2.

Our experimental study establishes that the single-phase 18-electron Heusler alloys with partial B2-type order in the as-cast state after arc melting are all Pauli paramagnetic metals, albeit with an enhanced temperature-independent susceptibility characteristic of the early 3*d* elements. Prolonged

annealing does not improve the atomic order, nor does it lead to the appearance of a (111) superstructure reflection that would herald the onset of ternary or quaternary atomic order. On the contrary, the quaternaries disproportionate irreversibly into more stable cubic phase mixtures, as predicted thermodynamically. The binaries do not develop full D0₃ order. There are corresponding small irreversible changes (~1%) in the Pauli susceptibility at the temperatures where disproportionation occurs.

More generally, future claims based on first-principles calculations for the discovery of new ternary and higher intermetallic phases with useful physical properties should be critically screened for stability, at least with respect to disorder and known competing phase mixtures on the hull. In this way, lengthy discussions of magnetic order and electronic structure of phases that do not exist could be avoided, as well as misidentification of small, irreversible features in the temperature-dependent susceptibility as Néel points. While disorder may improve the mechanical properties, it is inimical to collective magnetic order, which depends sensitively on local atomic arrangements and unusual structure in the electronic DOS.

Growth methods that avoid the melt, such as physical or chemical deposition on a substrate, might run a better chance of success. The opportunities for Fermi-level engineering and stabilizing unusual electronic or magnetic structures are wider for thin films with a surface on a substrate than they are for bulk crystalline materials. It is as thin films that new electronic materials are likely to be applied. However, computational complexity accumulates in three-slab first-principles calculations, and currently there is no hull for guidance.

ACKNOWLEDGMENTS

This work was supported by Science Foundation Ireland as part of the ZEMS contract 16/IA/4534. R.Z. acknowledges support from the China Scholarship Council. We are very grateful to Yangkun He for helpful discussions.

-
- [1] *Heusler Alloys: Properties, Growth, Applications*, edited by C. Felser and A. E. Hirohata (Springer, Heidelberg, 2016).
 - [2] F. Heusler, Über magnetische manganlegierungen, *Verh. Dtsch. Phys. Ges* **5**, 219 (1903).
 - [3] S. Skaftouros, K. Özdoğan, E. Şaşıoğlu, and I. Galanakis, Generalized Slater-Pauling rule for the inverse Heusler compounds, *Phys. Rev. B* **87**, 024420 (2013).
 - [4] J. Ma, V. I. Hegde, K. Munira, Y. Xie, S. Keshavarz, D. T. Mildebrath, C. Wolverton, A. W. Ghosh, and W. H. Butler, Computational investigation of half-Heusler compounds for spintronics applications, *Phys. Rev. B* **95**, 024411 (2017).
 - [5] J. Ma, J. He, D. Mazumdar, K. Munira, S. Keshavarz, T. Lovorn, C. Wolverton, A. W. Ghosh, and W. H. Butler, Computational investigation of inverse Heusler compounds for spintronics applications, *Phys. Rev. B* **98**, 094410 (2018).
 - [6] F. Kuroda, T. Fukushima, and T. Oguchi, First-principles study of magnetism and phase stabilities of V2 based antiferromagnetic Heusler alloys, *J. Appl. Phys.* **127**, 193904 (2020).
 - [7] S. Jiang and K. Yang, Review of high-throughput computational design of Heusler alloys, *J. Alloys Compd.* **867**, 158854 (2021).
 - [8] V. D. Buchelnikov, V. V. Sokolovskiy, O. N. Miroshkina, D. R. Baigutlin, M. A. Zagrebin, B. Barbiellini, and E. Lähderanta, Prediction of a Heusler alloy with switchable metal-to-half-metal behavior, *Phys. Rev. B* **103**, 054414 (2021).
 - [9] J. Balluff, K. Diekmann, G. Reiss, and M. Meinert, High-throughput screening for antiferromagnetic Heusler compounds using density functional theory, *Phys. Rev. Mater.* **1**, 034404 (2017).
 - [10] Q. Gao, I. Opahle, and H. Zhang, High-throughput screening for spin-gapless semiconductors in quaternary Heusler compounds, *Phys. Rev. Mater.* **3**, 024410 (2019).
 - [11] K. Özdoğan, E. Şaşıoğlu, and I. Galanakis, Slater-Pauling behavior in LiMgPdSn-type multifunctional quaternary Heusler materials: Half-metallicity, spin-gapless and magnetic semiconductors, *J. Appl. Phys.* **113**, 193903 (2013).
 - [12] X. Wang, Proposal for a New Class of Materials: Spin Gapless Semiconductors, *Phys. Rev. Lett.* **100**, 156404 (2008).

- [13] I. Galanakis, K. Özdoğan, and E. Şaşıoğlu, High- T_C fully compensated ferrimagnetic semiconductors as spin-filter materials: The case of CrVXAl ($X = \text{Ti, Zr, Hf}$) Heusler compounds, *J. Phys. Condens. Matter* **26**, 379501 (2014).
- [14] Y. Venkateswara, S. Gupta, S. S. Samatham, M. R. Varma, K. Suresh, and A. Alam, Competing magnetic and spin-gapless semiconducting behavior in fully compensated ferrimagnetic CrVTiAl : Theory and experiment, *Phys. Rev. B* **97**, 054407 (2018).
- [15] M. E. Jamer, B. Wilfong, V. D. Buchelnikov, V. V. Sokolovskiy, L. H. Lewis, A. Pulkkinen, B. Barbiellini, A. Bansil, and D. Heiman, Superconducting and antiferromagnetic properties of dual-phase V_3Ga , *Appl. Phys. Lett.* **117**, 062401 (2020).
- [16] L. Pendry and D. Douglass, Superconductivity of V_3Al , *Solid State Commun.* **18**, 177 (1976).
- [17] G. Y. Gao and K.-L. Yao, Antiferromagnetic half-metals, gapless half-metals, and spin gapless semiconductors: The D0_3 -type Heusler alloys, *Appl. Phys. Lett.* **103**, 232409 (2013).
- [18] I. Galanakis, Ş. Tırpancı, K. Özdoğan, and E. Şaşıoğlu, Itinerant G-type antiferromagnetism in D0_3 -type V_3Z ($Z = \text{Al, Ga, In}$) compounds: A first-principles study, *Phys. Rev. B* **94**, 064401 (2016).
- [19] M. E. Jamer, B. A. Assaf, G. E. Sterbinsky, D. Arena, L. H. Lewis, A. A. Saúl, G. Radtke, and D. Heiman, Antiferromagnetic phase of the gapless semiconductor V_3Al , *Phys. Rev. B* **91**, 094409 (2015).
- [20] G. M. Stephen, I. McDonald, B. Lejeune, L. H. Lewis, and D. Heiman, Synthesis of low-moment CrVTiAl : A potential room temperature spin filter, *Appl. Phys. Lett.* **109**, 242401 (2016).
- [21] Y. Qiu, Y. J. Hu, A. Taylor, M. J. Styles, R. K. W. Marceau, A. V. Ceguerra, M. A. Gibson, Z. K. Liu, H. L. Fraser, and N. Birbilis, A lightweight single-phase AlTiVCr compositionally complex alloy, *Acta Mater.* **123**, 115 (2017).
- [22] G. M. Stephen, G. Buda, M. E. Jamer, C. Lane, S. Kaprzyk, B. Barbiellini, D. Graf, L. H. Lewis, A. Bansil, and D. Heiman, Structural and electronic properties of the spin-filter material CrVTiAl with disorder, *J. Appl. Phys.* **125**, 123903 (2019).
- [23] G. M. Stephen, C. Lane, G. Buda, D. Graf, S. Kaprzyk, B. Barbiellini, A. Bansil, and D. Heiman, Electrical and magnetic properties of thin films of the spin-filter material CrVTiAl , *Phys. Rev. B* **99**, 224207 (2019).
- [24] D. Betto, N. Thiyagarajah, Y.-C. Lau, C. Piamonteze, M.-A. Arrio, P. Stamenov, J. M. D. Coey, and K. Rode, Site-specific magnetism of half-metallic $\text{Mn}_2\text{Ru}_x\text{Ga}$ thin films determined by x-ray absorption spectroscopy, *Phys. Rev. B* **91**, 094410 (2015).
- [25] Y. Takamura, R. Nakane, and S. Sugahara, Analysis of L2_1 -ordering in full-Heusler Co_2FeSi alloy thin films formed by rapid thermal annealing, *J. Appl. Phys.* **105**, 07B109 (2009).
- [26] J. M. D. Coey, *Magnetism and Magnetic Materials* (Cambridge University Press, Cambridge, 2010).
- [27] B. Childs, W. Gardner, and J. Penfold, The magnetic susceptibility of vanadium between 20 and 293 K, *Philos. Mag.* **4**, 1126 (1959).
- [28] E. Fawcett, Spin-density-wave antiferromagnetism in chromium, *Rev. Mod. Phys.* **60**, 209 (1988).
- [29] B. G. Childs, W. E. Gardner, and J. Penfold, The magnetic susceptibility of vanadium-chromium solid solutions, *Philos. Mag.* **5**, 1267 (1960).
- [30] B. G. Childs, W. E. Gardner, and J. Penfold, The magnetic susceptibilities of vanadium-based solid solutions containing titanium, manganese, iron, cobalt and nickel, *Philos. Mag.* **8**, 419 (1963).
- [31] J. Emsley, *The Elements* (Oxford University Press, Oxford, 1989).
- [32] E. Şaşıoğlu, Nonzero macroscopic magnetization in half-metallic antiferromagnets at finite temperatures, *Phys. Rev. B* **79**, 100406(R) (2009).
- [33] H. Kurt, K. Rode, P. Stamenov, M. Venkatesan, Y.-C. Lau, E. Fonda, and J. M. D. Coey, Cubic Mn_2Ga Thin Films: Crossing the Spin Gap with Ruthenium, *Phys. Rev. Lett.* **112**, 027201 (2014).
- [34] R. Stinshoff, A. K. Nayak, G. H. Fecher, B. Balke, S. Ouardi, Y. Skourski, T. Nakamura, and C. Felser, Completely compensated ferrimagnetism and sublattice spin crossing in the half-metallic Heusler compound $\text{Mn}_{1.5}\text{FeV}_{0.5}\text{Al}$, *Phys. Rev. B* **95**, 060410(R) (2017).
- [35] K. E. Siewierska, G. Atcheson, A. Jha, K. Esien, R. Smith, S. Lenne, N. Teichert, J. O'Brien, J. M. D. Coey, P. Stamenov, and K. Rode, Magnetic order and magneto-transport in half-metallic ferrimagnetic $\text{Mn,Ru}_x\text{Ga}$ thin films, *arXiv:2012.05736* (2020).
- [36] OpenMx, <http://www.openmx-square.org>.
- [37] G. Xu, E. Liu, Y. Du, G. Li, G. Liu, W. Wang, and G. Wu, A new spin gapless semiconductors family: Quaternary Heusler compounds, *Europhys. Lett.* **102**, 17007 (2013).
- [38] P. Cao, H. Zhao, S. Liu, F. Tian, and Y. Wang, Ordering induced transformation from high-entropy to Heusler CrVTiAl alloy, *Phys. Lett. A* **383**, 125934 (2019).
- [39] J.-W. Yeh, S.-K. Chen, S.-J. Lin, J.-Y. Gan, T.-S. Chin, T.-T. Shun, C.-H. Tsau, and S.-Y. Chang, Nanostructured high-entropy alloys with multiple principal elements: Novel alloy design concepts and outcomes, *Adv. Eng. Mater.* **6**, 299 (2004).
- [40] Y. Ye, Q. Wang, J. Lu, C. Liu, and Y. Yang, High-entropy alloy: Challenges and prospects, *Mater. Today* **19**, 349 (2016).
- [41] E. P. George, D. Raabe, and R. O. Ritchie, High-entropy alloys, *Nat. Rev. Mater.* **4**, 515 (2019).
- [42] S. Kirklin, J. E. Saal, B. Meredig, A. Thompson, J. W. Doak, M. Aykol, S. Rühl, and C. Wolverton, The open quantum materials database (OQMD): Assessing the accuracy of DFT formation energies, *npj Comput. Mater.* **1**, 15010 (2015).
- [43] J. E. Saal, S. Kirklin, M. Aykol, B. Meredig, and C. Wolverton, Materials design and discovery with high-throughput density functional theory: The open quantum materials database (OQMD), *JOM* **65**, 1501 (2013).